Supercapacitor-Based Embedded Hybrid Solar/Wind Harvesting System Architectures

Mohamadhadi Habibzadeh*, Moeen Hassanalieragh†, Tolga Soyata*, Gaurav Sharma†
*Department of Electrical and Computer Engineering, SUNY Albany, Albany, NY 12203
†Department of Electrical and Computer Engineering, University of Rochester, Rochester, NY 14627
{hhabibzadeh, tsoyata}@albany.edu*, {m.hassanalieragh, gurav.sharma}@rochester.edu†

***Abstract*—Off-grid medium-power (1–10 W) systems require either battery- or supercapacitor-based ambient energy harvesting for sustaining their operation. Supercapacitor-based harvesters are advantageous in autonomous field systems due to their extended lifetime, easy power management, and low maintenance requirement; however, they can reach only up to 10% of the energy density of rechargeable batteries. To overcome this energy density challenge, hybrid power sources, such as solar or wind, can be advantageously utilized in harvesting systems. The complementary power supply characteristics of solar and wind can substantially reduce the required supercapacitor buffer size compared with solar-only or wind-only systems. In the literature, no supercapacitor-based hybrid harvesting system design exists for 1–10 W range. In this paper, we develop and experimentally validate three different categories of supercapacitor-based harvesting systems that are capable of simultaneously harvesting solar/wind (hybrid) power sources.**

***Index Terms*—Hybrid energy harvesting; wind power harvesting; embedded systems; solar power harvesting.**

I. Introduction

For autonomous field systems that are based on intense computation in the field (e.g., wildlife monitoring [1] and smart cities [2], [3]), supercapacitor buffering is an emerging alternative to rechargeable batteries [4]–[6]. These systems require medium-range power (1–10 W) and a fairly large supercapacitor buffer due to the low energy density of supercapacitors. Typically, solar-only power input is used in these systems; however, the analysis conducted in [7] reveals that using a hybrid (solar/wind) harvester, the requirement for large supercapacitors can be eliminated due to the complementary availability of solar and wind power. While solar-only supercapacitor-based harvester designs exist for this power range, hybrid harvesters are confined into ultra low- and low-power ranges [8], [9] and few such systems are developed for medium-power applications. In this paper, we present three categories of hybrid harvester designs, elaborate on their circuit-level details, and provide experimental validations for a select set of these systems.

The rest of this paper is organized as follows. In Section II, we study the architecture of a typical hybrid energy harvester. In Section III, we introduce the three categories of our hybrid harvester designs. In Section IV, we provide detailed circuit level information about the components that make up these systems. In Section V, we provide experimental results of our systems. We conclude the paper by summarizing our research in Section VI.

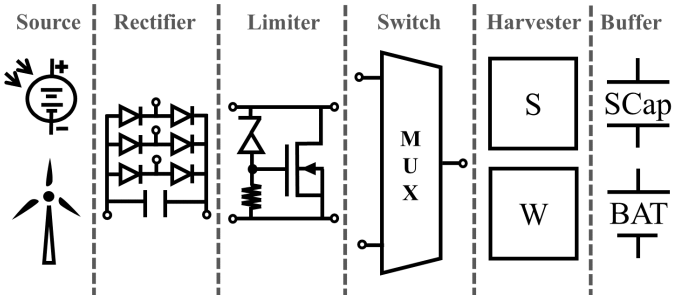

Figure 1: General architecture of an energy harvesting system, consisting of six components: source, rectifier, limiter, switch, harvester, and buffer.

II. Harvesting Systems

As detailed in [7], typical energy harvesters leverage the same architecture, which is depicted in Fig. 1. This architecture is composed of six components: source, rectifier, limiter, switch, harvester, and energy buffer. Our design strategy is to implement most of these components as add-on boards to enable a highly modular harvesting system design. These components are:

Source refers to the ambient power transducers (such as wind turbines and solar panels) that provide power to the system. **Rectifier** converts AC power to DC, which is only necessary if the power source provides an AC output (e.g., a wind turbine that provides three-phase AC power). A rectifier is not necessary for the solar panels, because they provide a DC output. **Limiter** provides over-voltage protection for other components of the system. While ultra-low and low power transducers typically require a voltage booster, due to their voltage levels being in the 1 V range, medium-power transducers (e.g., an embedded wind turbine) can produce 50–100 V outputs, exceeding the safe operating voltage range (e.g., 25–30 V) of the switch or the harvester that is connected to it, thereby requiring a voltage limiter. **Switch** allows the harvesting board to disconnect and reconnect to a power source either in a round robin fashion or based on its power availability. We detail the implementation of this component in Section IV.

Harvester controls the entire energy harvesting process by balancing the power of transducers, the charging/discharging power of the *Buffer* component, and the load. For efficient harvesting, the harvested power of each source is controlled by

a suitable Maximum Power Point Tracking (MPPT) algorithm, executed by the harvester firmware. This component can also provide over-power, over-voltage, and over-current protection to safeguard its internal circuit components and the energy buffer. Furthermore, it can provide services for data logging —for debugging and monitoring purposes— and communication —thorough Bluetooth, ZigBee, RS232, etc. Simple harvesters can be implemented on a PCB (which we refer to as harvesting board hereafter) using only passive circuit elements and a Pulse Width Modulation (PWM) circuit, which controls the flow of energy through its duty cycle [10]. Intelligent harvesters utilize microcontroller firmware to implement an MPPT algorithm. The example harvester component of Fig. 1 includes two harvesting boards; the letter S indicates that the firmware executes a solar power MPPT algorithm, whereas the letter W denotes that the harvester executes a wind MPPT algorithm. Among proposed MPPT algorithms for solar [11] and wind [12], we use fractional open circuit voltage [13] and Hill Climbing (HC) [14] for solar and wind MPPT, respectively. **Buffer** is used to guarantee continuous power availability, since ambient sources provide intermittent power; for example, solar panels do not generate power during night. The surplus portion of the harvested energy can be buffered in an energy buffer such as a battery or a supercapacitor block, which can be retrieved later when the load consumes higher instantaneous power than what is generated by the source.

III. Hybrid Energy Harvesting

In this section, we use the generic architecture shown in Fig. 1 to develop three hybrid energy harvesting systems that offer different tradeoffs among cost, power harvesting capability, extendibility, and fault tolerance. Our proposed systems are developed by combining and modifying the components of existing single-source, solar-only [15] and wind-only [16] harvesters.

A. Independent Hybrid Harvesting

The simplest form of hybrid energy harvesting systems can be implemented by operating solar-only (S) and wind-only (W) harvesters in parallel, where each power input has its own independent harvesting board. A shared supercapacitor energy buffer is used to buffer the surplus energy from both harvesters. We term this hybrid harvesting approach *Independent Hybrid Harvesting*, because each harvester operates independently form the other. Figure 2 depicts the high-level architecture of an independent solar/wind hybrid energy harvester (which we refer to as the SW configuration). We assume that the output voltage of the solar panel is within the operating range of the harvesting board that it is connected to; therefore, a voltage limiter is not required for the solar panel. In contrast, a limiter is used to keep the rectified voltage of the wind turbine within the safe range, as we assume that it can exceed this range. The S harvesting board executes a suitable MPPT algorithm for solar power (e.g., fractional open-circuit voltage MPPT), while the W harvester executes a wind MPPT algorithm (e.g., HC). Because there is no energy channeling from one source to more than one harvester, no switching mechanism is necessary.

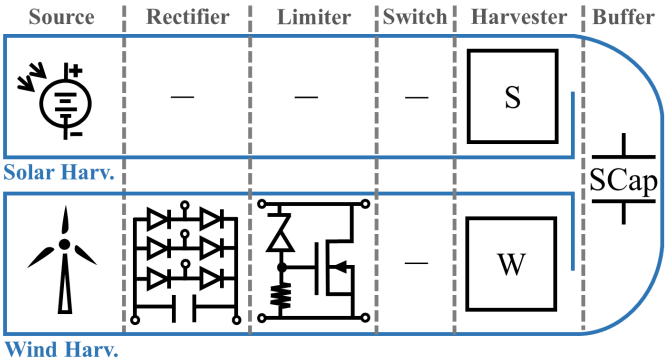

Figure 2: High-level architecture of the SW configuration. The voltage of the wind turbine is rectified and voltage-limited to prevent over-voltage in the harvester.

The main advantages of this architecture are its simplicity and expandability; additional S and W harvesters can be used to expand the configuration to three-input hybrid power sources, such as solar/solar/wind (SSW) and solar/wind/wind (SWW). For example, in the SSW configuration, placing two solar panels at different locations or orientations can create a hybrid solar power source, because solar irradiation —and the consequent generated solar power— can be vastly different and complementary [17]. For the same reason, SS —and WW— are also considered to be hybrid independent energy harvester configurations. Utilizing multiple independent solar-only and wind-only harvesters also contributes to the fault tolerance of the system; for example, a critical fault in the solar-only harvesting board (S) of the SWW configuration converts it to a WW harvester, thereby allowing the system to continue its operation, albeit with degraded performance. However, using one harvesting board for each power source increases size, weight, and cost, making it unsuitable for cost sensitive applications.

B. Cooperative Hybrid Harvesting

The lack of cooperation between the harvesting boards in the independent hybrid harvesting can lead to a low hardware utilization rate. For example, if the wind turbine in an SSW configuration generates a large amount of power during a night, its dedicated harvesting board (W) intentionally burns the excess portion of the power to provide over-power protection, while the two solar-only (S) boards are idle. This roughly translates to a 33% hardware utilization. We propose *Cooperative Hybrid Harvesting* to address this drawback. Figure 3 depicts the high level implementation of a cooperative solar/solar and a cooperative wind/solar harvester, which we refer to as S_2S_2 and S_2W_2, respectively. In cooperative hybrid harvesters, there is a dedicated harvesting board for each power source, which executes the suitable MPPT algorithm for that source. An analog multiplexer (MUX) for each harvesting board allows it to connect to —and to disconnect from— the power sources it is associated with. Furthermore, there is a communication channel between the cooperating harvesting

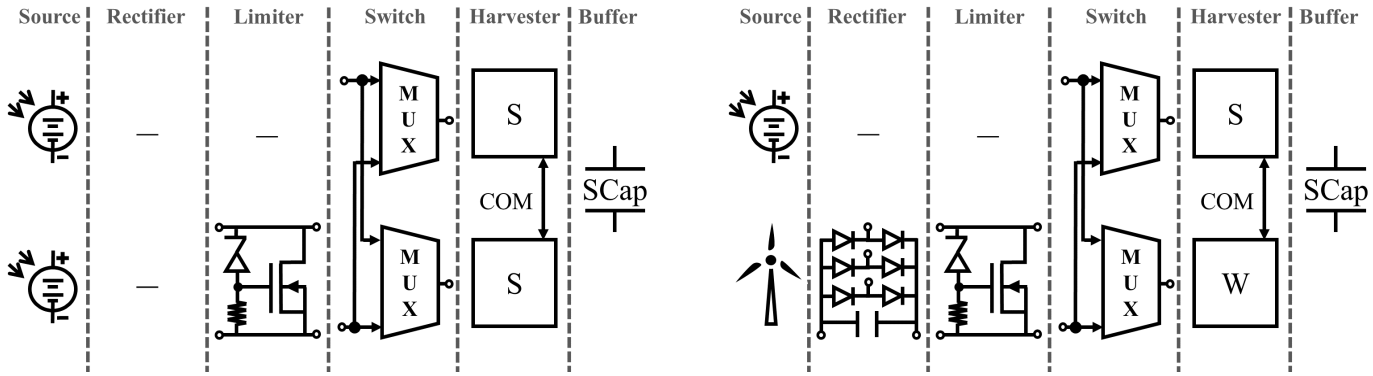

Figure 3: The S_2S_2 (left) and S_2W_2 (right) configurations of the cooperative harvesting system. In S_2S_2, two different solar panels are used; only the second one needs a voltage limiter. In S_2W_2, the wind turbine needs a rectifier and a voltage limiter.

boards (denoted as "COM" in Fig. 3), which allows them to coordinate their harvesting based on each other's status.

Assuming that each harvester has a power threshold limit of P_{limit}, the operation of cooperative and independent hybrid harvesters is identical as long as their input power level is below P_{limit}; in this case, no cooperation occurs between the harvesting boards. When the power level of a source exceeds P_{limit}, its dedicated harvesting board sends a help request to other harvesting board(s), which is either granted or denied, depending on the power level of the harvester that receives the help request; a harvester denies a help request if its own input power level is sufficient (i.e., it has sufficient energy to harvest), otherwise it grants the request (i.e., helping its requester will yield a higher aggregate power). In this configuration, each harvesting board operates in one of two modes: *independent* vs. *cooperative*, where the latter mode is entered into upon an established communication link. In cooperative mode, the requester assumes the *master* role, while the granter assumes the *slave* role. The slave board **(i)** halts the execution of its MPPT algorithm, **(ii)** disconnects its power source, and **(iii)** connects to the master board's power source by configuring its dedicated MUX. In the meantime, the master board executes its MPPT algorithm and shares its harvesting duty cycle (D_h) with the slave board over the communication channel. Since both boards use the same duty cycle, the power is distributed evenly between them. This allows a harvester to harvest up to $n \times P_{limit}$ Watts, when there are $n-1$ slave boards and one master board in a cooperation.

A USART module in a microcontroller is suitable for two-input configurations (e.g., S_2S_2 and S_2W_2 in Fig. 3). For $\geq$3-input configurations (e.g., $W_3W_3W_3$, $S_3W_3W_3$, and $S_3S_3W_3$), more advanced protocols such as SPI and CAN are needed.

C. Time-multiplexed Hybrid Harvesting

Independent and cooperative hybrid harvesters are not suitable for cost sensitive applications, because using a dedicated harvesting board for each power source increases system cost. We propose the *Time-Multiplexed Hybrid Harvesting* architecture to address this limitation. Figure 4 depicts the high-level implementation of two example configurations of this architecture: time-multiplexed solar/wind ($S||W$) and time-multiplexed solar/solar/wind ($S||S||W$). A careful observation of Fig. 4 shows that the harvester in this architecture must be capable of executing both solar and wind MPPT algorithms. There is a single n:1 analog MUX for n power sources. The harvesting board cycles through each power source in a time-based round robin fashion at the switching frequency of f_{sw}; at any point in time, only one source is connected to (for a duration of D_{sw}/f_{sw} seconds, assuming D_{sw} is the switching duty cycle), while $n-1$ of them are disconnected. While a source is disconnected, its generated power is buffered in *input buffer capacitors*, which are a part of the MUX design, as we detail in Section IV. Once reconnected, the harvesting board starts executing the MPPT algorithm of that source and soaks up the harvested energy —which is accumulated during the disconnection period— from the input buffer capacitor.

IV. Circuit Implementation

In this section, we detail the circuit design and operation of the architectural components illustrated in Fig. 1.

A. Rectifier

The voltage rectifier can be implemented using a conventional three-phase diode bridge rectifier [18].

B. Limiter

Circuit schematic of the voltage limiter is depicted in Fig. 4, under the "Limiter" component. When the input voltage reaches ≈25 V, the Zener diode is reverse-biased, turning on the N-channel MOSFET and allowing it to burn the excess power; this limits the voltage level at ≈25 V, when a 1N4749 Diode, 600 Ω resistor, and an IRFZ14 [19] MOSFET are used.

C. Switch

Figure 5 depicts the implementation of the analog MUX, used in the *Switch* component of the time-multiplexed hybrid harvesting. We use the same MUX in the cooperative hybrid harvesting as well; however, input buffer capacitors C_{in1} and C_{in2} are not necessary in this architecture. The analog MUX allows the embedded microcontroller to select one of the power sources —connected to terminals SRC1 or SRC2—

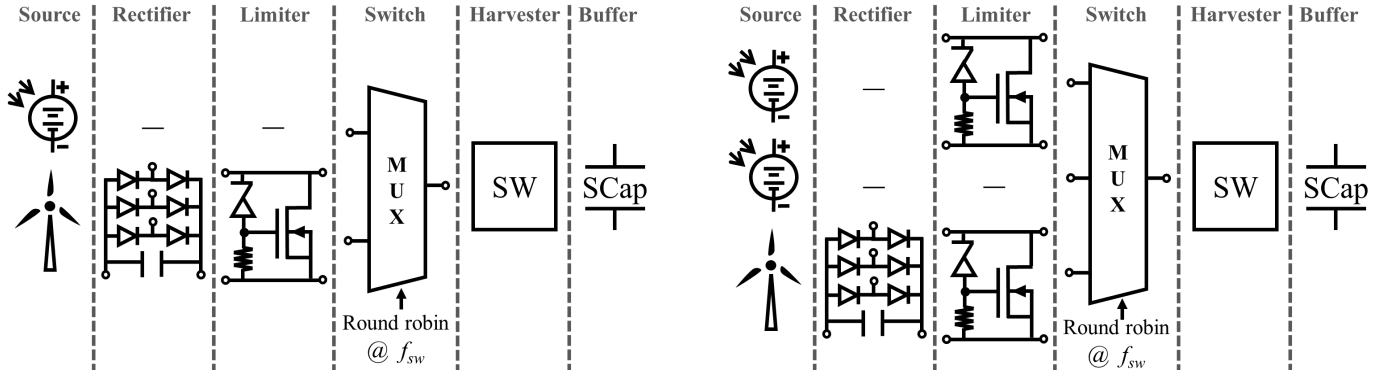

Figure 4: The $S||W$ (left) and $S||S||W$ (right) configurations of the time-multiplexed harvesting system category, requiring a 2:1 MUX and a 3:1 MUX, recpectively. One solar panel in $S||S||W$ is assumed to require a voltage limiter.

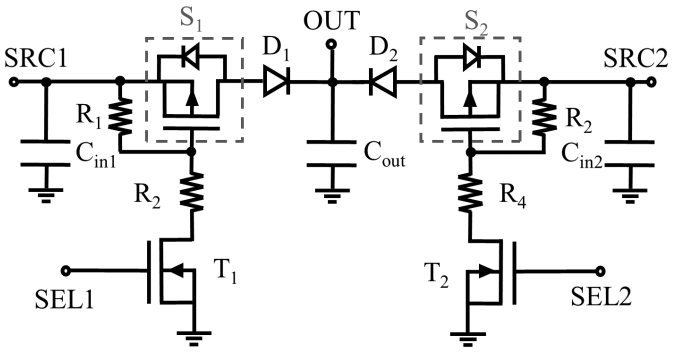

Figure 5: The analog multiplexer used in time-multiplexed and cooperative harvesting architectures; implemented using the following parts: $R_1 = 5.6\,k\Omega$, $R_2 = 2.5\,k\Omega$ $T_1 = T_2 = 2N7002$, $S_1 = S_2 = IRF9540N$, $D_1 = D_2 = SB560$, $C_{in1} = S_{in2} = 4700\,\mu F$.

by enforcing a 5 V voltage at the select terminals (SEL1 and SEL2) of the N-channel MOSFET (T_1 and T_2). For example, when a 5 V voltage is applied to the SEL1 terminal, T_1 turns on, which causes the S_1 gate-source voltage (V_{GS}) to be negative, thereby turning S_1 on and connecting SRC1 to OUT. D_1 and D_2 are used to prevent reverse current from output (OUT) to the inputs (SRC1, SRC2), when the supercapacitor voltage is higher than the power source voltage. A relatively small capacitor is used at the output (C_{out}) to filter high-frequency components caused by the MUX state transitions.

The configuration shown in Fig. 5 allows the analog MUX to act as an *energy MUX*, rather than a power MUX; the design goal of this circuit is to switch from one source of accumulated power (i.e., *energy*) to another, by using the input buffer capacitors C_{in1} and C_{in2}. In this section, we quantify min/max values of C_{in1} and C_{in2} for proper system operation.

Quantifying C_{in1}^{min} and C_{in2}^{min}: when a power source is disconnected from the harvesting board, the voltage increase (ΔV) of the capacitor during this period can be calculated as:

$$\Delta V = \frac{I_{SRC}}{C_{in1}} \times \frac{1 - D_{sw}}{f_{sw}}, \tag{1}$$

where I_{SRC} is the average current of SRC1, D_{sw} is the switching duty cycle, and f_{sw} is the MUX switching frequency. Assuming an initial capacitor voltage of V_{MPP1}, Eq. 1 implies that increasing the input buffer capacitance decreases voltage ripples around V_{MPP1}, which results in improved efficiency. We define these ripples as $\boxed{\text{MPP ripple} = \rho = \Delta V / V_{MPP1}}$, which allows us to calculate the minimum value of C_{in1} (C_{in1}^{min}) as follows:

$$C_{in1}^{min} = \frac{I_{SRC}}{\rho \cdot V_{MPP1}} \times \frac{1 - D_{sw}}{f_{sw}}. \tag{2}$$

Quantifying C_{in1}^{max} and C_{in2}^{max}: if the input buffer capacitor is very large, the convergence delay to V_{MPP} increases. We can find the max value of C_{in1} (C_{in1}^{max}) in terms of the expected changes in V_{MPP} (ΔV_{exp}) between two consecutive periods:

$$C_{in}^{max} = \frac{I_{OUT}}{\Delta V_{exp}} \times \frac{D_{sw}}{f_{sw}}. \tag{3}$$

Quantifying C_{out}: during the SRC2→SRC1 switching, $V_{C_{in1}}$ and $V_{C_{out}}$ transition to an equilibrium voltage (V_e) as follows:

$$\begin{cases} V_{C_{in1}} = V_{MPP1} + \Delta V \\ V_{C_{out}} = V_{MPP2} \end{cases} \Longrightarrow \begin{cases} V_{C_{in1}} = V_e, \\ V_{C_{out}} = V_e. \end{cases} \tag{4}$$

During this transition, while one capacitor loses energy, the other one gains the same amount of energy, implying voltage fluctuations due to switching activity. We define these fluctuations as $\boxed{\text{switching ripple} = \gamma = |V_e - V_{MPP1}| / V_{MPP1}}$. referring to Eq. 4:

$$\frac{1}{2} \cdot C_{in1} \cdot \left((V_{MPP1} + \Delta V)^2 - V_e^2 \right) = \frac{1}{2} \cdot C_{out} \cdot (V_e^2 - V_{MPP2}^2). \tag{5}$$

Solving for C_{out}/C_{in1}, we can rewrite Eq. 5 as:

$$\begin{aligned} \frac{C_{out}}{C_{in1}} &= \frac{\left(1 + 2 \cdot \rho + \rho^2\right) \cdot V_{MPP1}^2 - V_e^2}{V_e^2 - V_{MPP2}^2} \\ &\approx \frac{\left(1 + 2 \cdot \rho\right) \cdot V_{MPP1}^2 - (1 \mp 2 \cdot \gamma)^2 \cdot V_{MPP1}^2}{(1 \mp 2 \cdot \gamma)^2 \cdot V_{MPP1}^2 - V_{MPP2}^2} \end{aligned} \tag{6}$$

Defining $\boxed{\text{source MPP voltage ratio} = \lambda = V_{MPP2} / V_{MPP1}}$ allows us to re-write Eq. 6 as follows:

$$\frac{C_{out}}{C_{in1}} = \frac{2\rho \pm 2\gamma}{1 \mp 2\gamma - \lambda^2} = \begin{cases} \dfrac{2\rho + 2\gamma}{1 - 2\gamma - \lambda^2} & V_e > V_{MPP1} \\ \dfrac{2\rho - 2\gamma}{1 + 2\gamma - \lambda^2} & V_e < V_{MPP1} \end{cases} \tag{7}$$

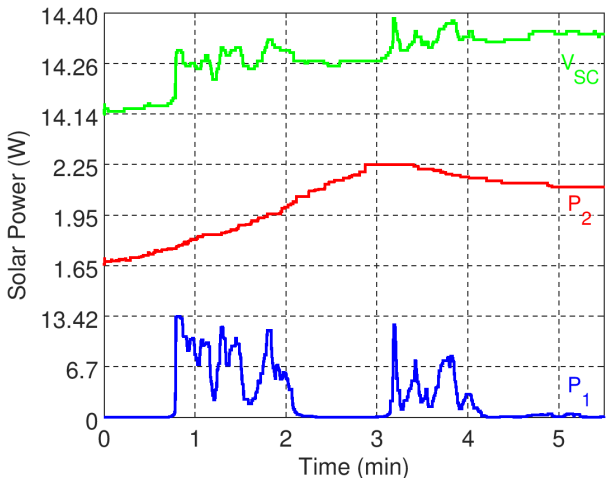

Figure 6: Two harvesting boards in an *SW* configuration, harvesting the same solar power source, cooperatively.

We conclude that the selection of the input and output capacitors in our analog MUX design is influenced by two design specifications, MPP ripple (ρ) and switching ripple (γ), as well as the MPP voltage ratio of the two input sources (λ), which are determined by environmental conditions.

D. Design Example

As a design example, let us assume that a 60 W power source, operating at $V_{MPP1} = 20$ V is connected to SRC1. We can deduce that $I_{SRC} = 3$ A. If we want the maximum tolerable MPP ripple to be 0.1 ($\rho \leq 0.1$), assuming that $I_{OUT} = 4$ A, $f_{sw} = 333$ Hz, and $D_{sw} = 0.5$, C_{in1}^{min} from Eq. 2 is:

$$C_{in1}^{min} = \frac{3}{0.1 \times 20} \times \frac{1 - 0.5}{333} = 2252\,\mu\text{F}. \tag{8}$$

Similarly, from Eq. 3, the C_{in1}^{max} for $\Delta V_{exp} = 0.5$ V is:

$$C_{in1}^{max} = \frac{4}{0.5} \times \frac{0.5}{333} = 12012\,\mu\text{F}. \tag{9}$$

If $V_{MPP2} = 12$ V, the source MPP ratio can be computed as $\lambda = 12/20 = 0.6$. Setting the maximum switching ripple to 6% ($\gamma = 0.06$) as our design goal, V_e would settle at $\approx$18.8 V ($V_e < V_{MPP1}$); we can use Eq. 7 to calculate C_{out}/C_{in1} as:

$$\frac{C_{out}}{C_{in}} = \frac{2 \times 0.1 - 2 \times 0.06}{1 + 2 \times 0.06 - 0.6^2} = 0.105, \tag{10}$$

$$\begin{cases} 2252\,\mu\text{F} \leq C_{in} \leq 12012\,\mu\text{F}, \\ 237\,\mu\text{F} \leq C_{out} \leq 1261\,\mu\text{F}, \end{cases} \tag{11}$$

In our experiments, we used C_{in}=4700μF and C_{out}=220μF.

V. Evaluation

We conducted multiple experiments to assess the functionality of our hybrid harvesters. In this section, we detail our experimental setup and discuss the experimental results for representative configurations of the proposed architectures.

A. Experimental Setup

We used UR-SolarCap [15] as the basis of our implementation. It is an open source solar-only energy harvester for medium-power applications. Its modular design allows it to be employed in all of the architectures we propose. Furthermore, its embedded measurement and communication modules provide real time monitoring of critical harvester parameters, such as instantaneous voltage and current of each power source and the supercapacitor block voltage. We developed a new firmware for UR-SolarCap, which executes the HC MPPT algorithm, thereby allowing it to be used as a wind energy harvester [16]. Our experimental setup consisted of a Higoo™ 50 W, 12 V_{rms} as our wind turbine and two 30 W solar panels connected in parallel (60 W total) as the solar source. The energy buffer was implemented by employing eight serially-connected 3000 F supercapacitors. As the maximum voltage of each supercapacitor is 2.7 V, the voltage of the block cannot exceed $8 \times 2.7 = 21.6$ V.

B. Independent Hybrid Harvesting

Because the operation of various configurations of the independent hybrid harvesting is similar, we only provide experimental results for the *SW* as the representative configuration of this category. The experimental results are shown in Fig. 6, where two harvesting boards, *Board1* and *Board2*, harvested from a wind turbine and a solar panel, respectively. During the $\approx$ 5.5-minute time interval of this experiment, the wind turbine delivered an average power of 2.5 W and the solar panel produced an average power of 2.0 W; the energy accumulation caused the supercapacitor voltage to rise from 14.14 V to 14.39 V, corresponding to a 1337 Joule energy increase in 330 s (an average power of 4.05 W). The difference between the buffered average power and the aggregate power input is due to the harvester efficiency $\left(\frac{4.05}{2.0 + 2.5} = 90\%\right)$.

C. Cooperative Hybrid Harvesting

We selected the S_2S_2 and W_2W_2 as the representative configurations of the cooperative harvesting architecture. The results are shown in the left and right side of the Fig. 7, respectively. The experiment for S_2S_2 was conducted for a time interval of $\approx$5 minutes, during which both harvesting boards cooperatively harvested the same solar panel. In this experiment, the solar panel delivered an average power of 7.3 W, out of which Board1 harvested $\approx$3.6 W and Board2 harvested $\approx$3.7 W, translating to a 49% and 51% load split. Supercapacitor voltage rose from 17.45 V to 17.77 V during the experiment, translating to a 2113 Joule energy accumulation in 330 s (6.4 W average power). Therefore, the harvester efficiency is $\left(\frac{6.45}{3.6 + 3.7} = 88\%\right)$.

The experiment for W_2W_2 conducted in a $\approx$50-minute interval, where both boards cooperatively harvested the same wind turbine and other wind turbine was left disconnected. During this experiment, the wind turbine delivered an average power of 1.10 W, out of which Board1 harvested $\approx$0.49 W and Board2 harvested $\approx$0.61 W, translating to a 45% and

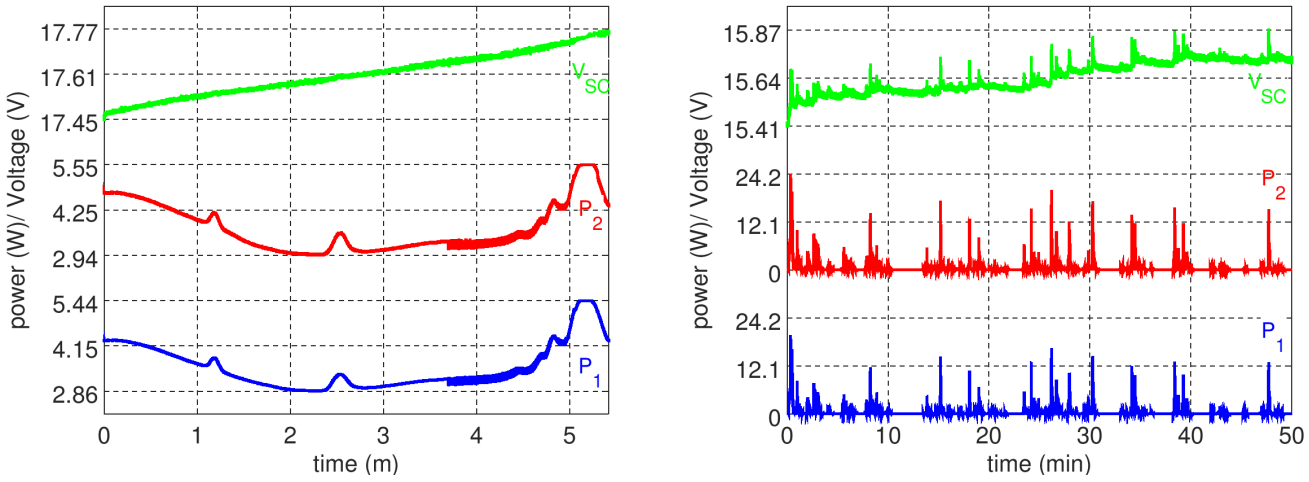

Figure 7: The diagram on the left shows the experimental results for an S_2S_2 configuration, whereas the one on the right shows the performance of a W_2W_2 harvester.

55% power split. In the worst case, Board1 harvested an instantaneous power of 19.4 W, while Board2 harvested an instantaneous power of 24.2 W, which corresponds to a power share of 44% and 56%. During the harvesting interval, the supercapacitor voltage rose from 15.41 V to 15.87 V, corresponding to 2698 Joules (0.90 W average power). Therefore, the harvester efficiency is $\left(\frac{0.90}{0.49+0.61} = 81\%\right)$.

VI. Conclusions

In this paper, we propose multiple hybrid (solar/wind) energy harvester designs for medium-power applications, which provide trade-offs among power harvesting capability, fault tolerance, cost, and expandability. We base our designs on an open-source solar-only harvester and present our hybrid designs in three categories: i) independent hybrid harvesters work by connecting the output of multiple independent harvesters into the same energy buffer, ii) cooperative harvesters allow harvesting hybrid sources using multiple harvesters that communicate over a communication channel, and iii) time-multiplexed hybrid harvesters operate by harvesting individual power sources in dedicated time intervals. We experimentally demonstrate the functionality of the first two categories.

References

[1] A. Mainwaring, D. Culler, J. Polastre, R. Szewczyk, and J. Anderson, "Wireless sensor networks for habitat monitoring," in *ACM Int. Wkshp on Wireless Sensor Net. and App.* Acm, 2002, pp. 88–97.

[2] M. Habibzadeh, Z. Qin, T. Soyata, and B. Kantarci, "Large Scale Distributed Dedicated- and Non-Dedicated Smart City Sensing Systems," *IEEE Sensors Journal*, 2017, Accepted for Publication.

[3] M. Habibzadeh, W. Xiong, M. Zheleva, E. K. Stern, B. H. Nussbaum, and T. Soyata, "Smart City Sensing and Communication Sub-Infrastructure," in *IEEE Midwest Synmposium on Circuits and Systems*, Boston, MA, Aug 2017.

[4] F. I. Simjee and P. H. Chou, "Efficient charging of supercapacitors for extended lifetime of wireless sensor nodes," *IEEE Transactions on Power Electronics*, vol. 23, no. 3, pp. 1526–1536, May 2008.

[5] D. Brunelli, C. Moser, L. Thiele, and L. Benini, "Design of a solar-harvesting circuit for batteryless embedded systems," *IEEE TCAS I: Regular Papers*, vol. 56, no. 11, pp. 2519–2528, Nov 2009.

[6] M. Hassanalieragh, T. Soyata, A. Nadeau, and G. Sharma, "Solar-Supercapacitor Harvesting System Design for Energy-Aware Applications," in *Proceedings of the 27th IEEE International System-on-Chip Conference (IEEE SOCC)*, Las Vegas, NV, Sep 2014, pp. 280–285.

[7] M. Habibzadeh, M. Hassanalieragh, A. Ishikawa, T. Soyata, and G. Sharma, "Hybrid Solar-Wind Energy Harvesting for Embedded Applications: Supercapacitor-based System Architectures and Design Tradeoffs," *IEEE Circuits and Systems Magazine (MCAS)*, 2018, Accepted for Publication.

[8] N. Kong and D. S. Ha, "Low-Power Design of a Self-powered Piezoelectric Energy Harvesting System With Maximum Power Point Tracking," *IEEE TPEL*, vol. 27, no. 5, pp. 2298–2308, May 2012.

[9] T. Soyata, L. Copeland, and W. Heinzelman, "RF Energy Harvesting for Embedded Systems: A Survey of Tradeoffs and Methodology," *IEEE Circuits and Systems Magazine*, vol. 16, no. 1, pp. 22–57, Feb 2016.

[10] J. H. R. Enslin, M. S. Wolf, D. B. Snyman, and W. Swiegers, "Integrated photovoltaic maximum power point tracking converter," *IEEE Transactions on Ind. Elec.*, vol. 44, no. 6, pp. 769–773, Dec 1997.

[11] B. Subudhi and R. Pradhan, "A Comparative Study on Maximum Power Point Tracking Techniques for Photovoltaic Power Systems," *IEEE Transactions on Sustainable Energy*, vol. 4, no. 1, pp. 89–98, Jan 2013.

[12] Y. Zhao, C. Wei, Z. Zhang, and W. Qiao, "A Review on Position/Speed Sensorless Control for Permanent-Magnet Synchronous Machine-Based Wind Energy Conversion Systems," *IEEE JESTPE*, vol. 1, no. 4, pp. 203–216, Dec 2013.

[13] J. J. Schoeman and J. D. v. Wyk, "A Simplified Maximal Power Controller for Terrestrial Photovoltaic Panel Arrays," in *Power Electronics Specialists conference, 1982 IEEE*, June 1982, pp. 361–367.

[14] E. Koutroulis, K. Kalaitzakis, and N. C. Voulgaris, "Development of a Microcontroller-based, Photovoltaic Maximum Power Point Tracking Control System," *IEEE TPEL*, vol. 16, no. 1, pp. 46–54, Jan 2001.

[15] M. Hassanalieragh, T. Soyata, A. Nadeau, and G. Sharma, "UR-SolarCap: An Open Source Intelligent Auto-Wakeup Solar Energy Harvesting System for Supercapacitor Based Energy Buffering," *IEEE Access*, vol. 4, pp. 542–557, Mar 2016.

[16] M. Habibzadeh, M. Hassanalieragh, T. Soyata, and G. Sharma, "Solar/Wind Hybrid Energy Harvesting for Supercapacitor-based Embedded Systems," in *IEEE Midwest Synmposium on Circuits and Systems*, Boston, MA, Aug 2017.

[17] H. Mousazadeh, A. Keyhani, A. Javadi, H. Mobli, K. Abrinia, and A. Sharifi, "A review of principle and sun-tracking methods for maximizing solar systems output," *Renewable and Sustainable Energy Reviews*, vol. 13, no. 8, pp. 1800 – 1818, 2009.

[18] M. Sakui and H. Fujita, "An analytical method for calculating harmonic currents of a three-phase diode-bridge rectifier with DC filter," *IEEE Transactions on Power Elec.*, vol. 9, no. 6, pp. 631–637, Nov 1994.

[19] "IRFZ14 Datasheet," http://www.vishay.com/docs/91289/91289.pdf.